Solvent-dependent Turn-on Probe for Dual Monitoring of Ag+ and Zn2+ in Living Biological Samples

ARTICLE *in* ANALYTICA CHIMICA ACTA · APRIL 2015

Impact Factor: 4.51 · DOI: 10.1016/j.aca.2015.01.052

7 AUTHORS, INCLUDING:

Bing Yin

Northwest University

36 PUBLICATIONS **382** CITATIONS

SEE PROFILE

Likai Hao

Eberhard-Karls-University Tuebingen

15 PUBLICATIONS **93** CITATIONS

SEE PROFILE

Ping Liu

Northwest University

63 PUBLICATIONS **1,071** CITATIONS

SEE PROFILE

Analytica Chimica Acta 868 (2015) 53–59

Contents lists available at ScienceDirect

Analytica Chimica Acta

journal homepage: www.elsevier.com/locate/aca

Solvent-dependent turn-on probe for dual monitoring of Ag^+ and Zn^{2+} in living biological samples

Zheng Yang [a,1], Mengyao She [a,1], Bing Yin [a,c], Likai Hao [b], Martin Obst [b], Ping Liu [a,*], Jianli Li [a,*]

[a] Ministry of Education Key Laboratory of Synthetic and Natural Functional Molecule Chemistry, College of Chemistry & Materials Science, Northwest University, Xi'an, Shaanxi 710069, PR China
[b] Center for Applied Geoscience, Institute for Geoscience, Eberhard Karls University Tuebingen, Hoelderlinstr. 12, Tuebingen 72074, Germany
[c] College of Chemistry, Beijing Normal University, No. 19, XinJieKouWai St., HaiDian District, Beijing 100875, PR China

HIGHLIGHTS

- A solvent-dependent probe was presented for dual monitoring of Ag^+ and Zn^{2+}.
- The probe exhibited special selectivity and sensitivity at physiological range.
- The mechanism was investigated both experimentally and computationally.
- The probe was highly suitable for mapping Ag^+ and Zn^{2+} in biological samples.

GRAPHICAL ABSTRACT

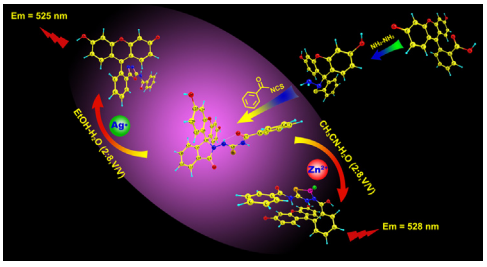

ARTICLE INFO

Article history:
Received 31 July 2014
Received in revised form 29 October 2014
Accepted 14 January 2015
Available online 7 February 2015

Keywords:
Fluorescence
Probe
Mechanism
DFT calculation
Bio-imaging

ABSTRACT

A novel, solvent-dependent "off–on" probe with benzoylthiourea moiety as the functional receptor and fluorescein as the fluorophore was designed for monitoring of Ag^+ in EtOH–H_2O (2:8, v/v) solution and Zn^{2+} in CH_3CN–H_2O (2:8, v/v) solution at physiological range with sufficient selectivity and sensitivity. The Ag^+ promoted desulfurization of thiosemicarbazide functionality in formation of the 1,3,4-oxadiazole and the coordination of Zn^{2+} to the O atom and N atom of the spoirolactam moiety and the S atom of the benzoylthiourea moiety were investigated to be the power that promoted the fluorescent enhancement. This probe was tested highly suitable for mapping Ag^+ and Zn^{2+} in living human osteosarcoma MG-63 cells and microbial cell–EPS–mineral aggregates, thus, providing a wonderful candidate for tracking Ag^+ and Zn^{2+} in biological organisms and processes.

1. Introduction

The design of fluorescent sensors with high sensitivity and selectivity for the quantification of heavy and transition metal ions in biological samples is challenging and an active subdiscipline of analytical chemistry [1–4]. Among a variety of investigated ions, special attentions have been devoted to Ag^+ and Zn^{2+}, due to their significant roles in environmental science, biology, medicine, and

* Corresponding authors. Tel.: +86 29 88302604; fax: +86 29 88302601.
E-mail addresses: liuping@nwu.edu.cn (P. Liu), lijianli@nwu.edu.cn (J. Li).
[1] These authors contributed equally to this work.

http://dx.doi.org/10.1016/j.aca.2015.01.052
0003-2670/

imaging industry [5–8]. To date, there are many reported sensors for Ag^+ and Zn^{2+}, respectively [9–13]. However, relatively few dual functional sensors for both Ag^+ and Zn^{2+} have been seen in literature. Additionally, since Ag^+ belongs to the so called "silent ions" which generally acts as a fluorescence quencher, most of the reported Ag^+ sensors were "on–off" type [14,15], i.e., fluorescence is eliminated/weakened by the ion, in contrast to "off–on" type, i.e., fluorescence is induced/enhanced in the presence of the ion, which in most cases is advantageous. As a result, there are strong needs for environmental applicable diagnostic dual functional "off–on" sensors for selective detection of both Ag^+ and Zn^{2+} in environmental and biological samples.

Fluorescent probes in combination with confocal microscopy are powerful tools due to the high sensitivity, non-destructive and fast analysis with spatial resolution [16–19]. In general, to obtain an excellent sensor, high specificity must be priority considered. However, a frequently encountered problem is that the application of the sensors is sometimes limited by the simplex binding property due to the noteworthy background interference caused by the complicated biological and environmental conditions. As a result, multifunctional probes that can be modulated in their selectivity to different ions with a change in media, are advantageous and highly desirable for applications [20,21]. In 2011, Liu et al. [22] firstly reported a rhodamine based dual-function probe which displayed high selectivity and extremely high sensitivity for Cu^{2+} in 9:1 (v/v) MeCN–H_2O mixed solvent and for ClO^- in 7:3 (v/v) MeOH–H_2O mixed solvent. Whereafter, a versatile rhodamine-based chemosensor that can sensitively and selectively recognize Cu^{2+} in the mixed solvent of DMSO–H_2O (v/v = 10:1) and Zn^{2+} in the mixed solvent of EtOH–H_2O through an off–on fluorescence emission was also presented by Xu et al. [23]. At present, there is an intense demand for new efficient multifunction chemosensors. Works related to this area are of significantly challenge and interest.

Fluorescein is a well-known and valuable fluorophore in the construction of fluorescent sensors, with excellent photophysical properties such as long wavelength excitation and emission profiles, large extinction coefficient and high fluorescence quantum yields [24]. Furthermore, the thiourea group is an ideal receptor with prominent attributes for thiophilic metal ion [25–27] including Cu^{2+}, Hg^{2+}, Fe^{3+}, Ag^+, and Zn^{2+}. In combination with a fluorescence probe, it is believed to have the potential to improve the stability of the probe while providing more binding positions, thus potentially improving the selectivity and fluorescent properties.

With these criteria in mind, herein, we present the design, synthesis, fluorescent properties and biological applications of a convenient fluorescent probe **1**, in which benzoylthiourea was chosen as the receptor and fluorescein as the fluorophore (Fig. S1). Probe **1** demonstrated excellent selective "off–on" responses toward Ag^+ in EtOH–H_2O (2:8, v/v) solution and Zn^{2+} in CH_3CN–H_2O (2:8, v/v) solution in the pH range of 6–9 (Figs. S2 and S3) with different recognition mechanisms where neither ion interferes with each other. This enable facile identification of each ones in the presence of the other. The probe has been used to visualize Ag^+/Zn^{2+} in living cells and microbial cell–EPS–mineral aggregates.

2. Experimental

2.1. General methods and reagents

Fluorescent spectra measurements were performed on a Hitachi F-4500 fluorescence spectrophotometer. The Elemental analyses were measured on a Vario EL III analyzer. NMR spectra were recorded on the Varian Inova-400 MHz spectrometer (at 400 MHz for ^1H and 100 MHz for ^{13}C) by using tetramethylsilane (TMS) as internal standard. High resolution mass spectra were performed on the Bruker micrOTOF-Q II ESI-Q-TOF LC/MS/MS Spectroscopy. IR spectra were performed on the Bruker Tensor 27 spectrometer. X-ray crystal data were collected on the Bruker Smart APEX II CCD diffractometer. The cell imaging experiments were performed on an Olympus FV1000 confocal microscope. The mapping Ag^+ and Zn^{2+} sorption to bacteria–EPS–mineral aggregate was did with Glovebox GP (concept) T4, Stereomicroscope and upright Confocal Laser Scanning Microscope Leica SPE, 4 lasers (405 nm, 488 nm, 561 nm, 635 nm) and 1 channel (variable spectral detection range).

The chemicals and reagents were all obtained from Sigma–Aldrich Co. LLC. Analytical thin layer chromatography was performed using Merck 60 GF254 silica gel (precoated sheets, 0.25 mm thick). Silica gel (0.200–0.500 mm, 60 A, J&K Scientific Ltd.) was used for column chromatography.

2.2. Synthesis of probe *1*

Fluorescein hydrazide was synthesized according to the references [28]. mp: 283–284 °C. Anal. calcd. for $C_{20}H_{14}N_2O_4$: H: 4.07, C: 69.36, N: 8.09. Found: H: 4.05, C: 69.39, N: 8.08. ^1H NMR (400 MHz, DMSO-d_6, TMS): d: 9.82 (s, 2H), 7.78 (d, J = 6.2 Hz, 1H), 7.48 (s, 2H), 6.99 (d, J = 7.0 Hz, 1H), 6.59 (s, 2H), 6.43 (dd, J = 20.9, 8.6 Hz, 4H). ^{13}C NMR (100 MHz, DMSO-d_6, TMS): d: 165.8, 158.4, 152.6, 151.7, 132.8, 129.5, 128.3, 123.6, 122.6, 112.2, 110.1, 102.6, 64.9. IR (KBr, υ cm^{-1}): 3310, 1691, 1612, 1506, 1468, 1368, 1320, 1238, 1182, 1111, 1044, 995, 843, 758, 690. MS (ESI) m/z = 345.0966 $[M-H]^-$, calc. for $C_{20}H_{14}N_2O_4$ = 346.0954.

Synthesis of **1**: fluorescein hydrazine (3.46 g, 0.01 mol) was dissolved in 50 mL ethanol and the benzoyl isothiocyanate (1.35 mL, 0.01 mol) were added to the solution in 20 min. The reaction mixture was then refluxed for 12 h. After cooling to the room temperature, the solvent was evaporated and then recrystallized from ethyl acetate to get the light yellow powder (3.06 g, yield: 60%). mp 262–263 °C. Anal. calcd for $C_{28}H_{19}N_3O_5S$: H, 3.76; C, 66.00; N, 8.25; S, 6.26, found: H, 3.77; C, 65.93; N, 8.27; S, 6.26. IR (KBr, υ cm^{-1}): 3442, 2970, 2873, 1685, 1608, 1508, 1462, 1442, 1345, 1307, 1224, 1176, 1110, 997, 925, 850, 761, 725, 694. ^1H NMR (400 MHz, DMSO-d_6, TMS) δ = 11.73 (d, J = 18.4 Hz, 2H), 9.98 (s, 2H), 7.94 (d, J = 7.2 Hz, 1H), 7.83 (d, J = 8.0 Hz, 2H), 7.71–7.59 (m, 3H), 7.47 (t, J = 7.4 Hz, 2H), 7.17 (d, J = 7.4 Hz, 1H), 6.56 (dd, J = 40.5, 18.2 Hz, 6H). ^{13}C NMR (100 MHz, DMSO-d_6, TMS) δ = 182.40, 168.36, 163.12, 158.90, 152.69, 150.69, 134.11, 133.37, 131.48, 129.27, 128.85, 128.35, 124.16, 123.27, 112.32, 107.83, 102.28, 65.40, 65.00 ppm. MS (ESI) calcd. for $C_{28}H_{19}N_3O_5S$: 509.1045, found: 508.1100 ($[M-H]^-$). Crystal data and structure refinement for **1**: $[C_{29}H_{20}Cl_3N_3O_6S]$; Mr = 644.89; size: 0.34 × 0.27 × 0.15 mm^3; monoclinic; T = 296 (2) K; space group *P2(1)/n*; a = 11.068(3) Å (11), b = 17.328(5) Å, c = 15.262(5) Å; α = 90.00°, β = 92.205(5)°, γ = 90.00°; V = 2924.9 (15) $Å^3$; Z = 4; Dc = 1.464 Mg m^{-3}, μ = 0.433 mm^{-1}; F(0 0 0) = 1320; theta range for data collection: 1.78–25.35°; reflections collected = 14300; independent reflections = 5300 (R_{int} = 0.0462); full-matrix least-squares refinement on F^2; goodness-of-fit on F^2 = 0.984; final R_1 = 0.1189 ($I > 2\sigma(I)$), wR_2 = 0.3841 ($I > 2\sigma(I)$); R indices (all data) R_1 = 0.1471 (all data), wR_2 = 0.4246 (all data); largest diff. peak and hole = 2.075 and −1.198 e$Å^{-3}$.

2.3. General procedure

Sensor **1** stock solution (500 μM): in a 25 mL volumetric flask, 0.07774 g **1** was dissolved in acetone and diluted to the mark. To two 100 mL volumetric tubes, 8.00 mL of the above solution was added to each volumetric tubes and diluted to the mark with EtOH–H_2O (2:8, v/v) solution and CH_3CN–H_2O (2:8, v/v) solution, respectively. The solutions of the ions were performed with the

salts including LiCl, NaCl, KCl, $AgNO_3$, $BaCl_2{\cdot}2H_2O$, $CaCl_2$, $MgCl_2{\cdot}6H_2O$, $CuCl_2{\cdot}2H_2O$, $FeCl_2$, $HgCl_2$, $NiCl_2{\cdot}6H_2O$, $PbCl_2$, $CdCl_2$, $MnCl_2{\cdot}5H_2O$, $ZnCl_2{\cdot}6H_2O$, $FeCl_3$, $CrCl_3$, $CoCl_2{\cdot}6H_2O$, $SnCl_4$, $AlCl_3$ in EtOH–H_2O (2:8, v/v) solution and CH_3CN–H_2O (2:8, v/v) solution, respectively. The solutions were prepared as 2.5 mM. Double distilled water was used throughout the experiments.

For determination of the spectra properties of **1**, 1.00 mL 0.2 M PBS, 0.50 mL of the 500 μM solution of **1** different concentration of Ag^+ and Zn^{2+} were added to the 25 mL volumetric tubes and diluted to the mark with EtOH–H_2O (2:8, v/v) solution and CH_3CN–H_2O (2:8, v/v) solution, respectively. The fluorescence intensity was recorded at 525 nm and 528 nm, respectively.

2.4. Crystal growth and conditions

White single crystal of the probe was obtained at room temperature from the mixed solvents of DMSO–ethanol solution by slow evaporation and then mounted on the goniometer of single crystal diffractometer. The crystal data have been collected at 296 K by using Mo Kα radiation by using ϕ/ω scan mode and collected for Lorentz and polarization effect (SADABS). The structure was solved using the direct method and refined by full-matrix least-squares fitting on F^2 by SHELX-97.

2.5. Computation details

The calculations of all the structures were performed with PBE1PBE [29] function via Gaussian 09 Program [30]. Probe **1** was optimized with a combination of basis of double-ζ quality consisting of 6-31G** for C, H elements, 6-31 + G* for N, O elements. Complex **2** (S_0 and S_1 state) was optimized with a combination of basis of double-ζ quality consisting of 6-31G** for C, H elements, 6-31 + G* for N, O elements. The possible structures of the complex **3** (S_0 and S_1 state) was optimized with a combination of basis of double-ζ quality consisting of 3-21G** for C, H elements, 3-21 + G* for S, N, O, and SVP for Zn element. All the optimized structures were confirmed to be local minimums due to the non-existence of imaginary frequency. Frequency analysis was not performed for excited state on account of the exhausting numerical calculation of the force constant for such a large system. The environmental effect of **2** was via PCM model with ethanol as the solvent molecule and CPCM model for **3**.

2.6. Fluorescent imaging in living cells

Human Osteosarcoma MG-63 cells were cultured in Dulbecco's Modified Eagle Medium (DMEM) supplemented with 10% FBS, at 37 °C in the humidified atmosphere with 5% CO_2 and 95% air. The cells were then cultured for 2 h until they plated on glass-bottomed dishes. The growth medium was then removed and the cells were washed with DMEM without FBS and incubated with 10 μM of the probes for 30 min at 37 °C, washed three times with PBS and imaged. Then the cells were supplemented with 2 equiv. of Ag^+ and 8% C_2H_5OH or 5 equiv. Zn^{2+} and 8% CH_3CN in the growth medium for 30 min at 37 °C, washed three times with PBS and imaged [31]. The fluorescence emissions were collected in the range of 515–545 nm with excitation wavelength at 488 nm.

2.7. Visualize silver and zinc sorption to microbial cell–EPS–mineral aggregates

The pure culture of phototrophic Fe(II)-oxidizing bacterium *Rhodobacter* sp. strain SW2 was prepared according to previous description. When 50 μM $AgNO_3/ZnCl_2$ were loaded for equilibration 12 h and a subsequent incubation with **1** in 8% C_2H_5OH/CH_3CN for 2 h, respectively. For bacterial cells and EPS labeling, SYTOX® Blue/SYTO® 9 green fluorescent nucleic acid stain and polysaccharide-specific *Arachis hypogaea* (peanut), Alexa Fluor® 568Conjugate/Wheat germ agglutinin, Alexa Fluor® 633 conjugate were added sequentially and incubation for 1 h, respectively [32,33] and then imaged with a Leica SPE confocal laser scanning microscope system.

3. Results and discussion

To verify the selectivity to metal ions, **1** was treated with a variety of metal ions including Li^+, Na^+, K^+, Ag^+, Mg^{2+}, Ca^{2+}, Ba^{2+}, Mn^{2+}, Co^{2+}, Ni^{2+}, Cu^{2+}, Zn^{2+}, Pb^{2+}, Cd^{2+}, Hg^{2+}, Al^{3+}, Cr^{3+}, Fe^{3+}, and Sn^{4+} in aqueous mixed solvents. Originally, **1** displays colorless and non-fluorescent in the absence of metal ions. While in EtOH–H_2O mixed solution, upon addition 2.0 equiv. of Ag^+, a significant change at 525 nm was observed. Solution investigation suggested that the ratios of EtOH to water obviously affected the response of probe **1** to Ag^+ and the EtOH–H_2O (2:8, v/v) mixed solution would be the optimum since the pure solution of water and EtOH both caused negligible fluorescence changing. Time dependent study showed that the reaction of **1** and Ag^+ completed rapidly within 1 s (Fig. S12). The additional Zn^{2+} induced a weak response, whereas other metal ions showed insignificant responses (Fig. 1a). In addition, although Hg^{2+} is well-known for desulfuerization reaction of thiosemicarbazide group, it is clear that the addition of Hg^{2+} induced quite weak response within a short period of time (Fig. S13), which was observably inferior compared with Ag^+. Thus, it can be concluded that the existence of Hg^{2+} showed insignificantly interference to the selectivity of probe **1** to Ag^+, indicating the high specificity of the probe for Ag^+. A linear relationship was found between the concentration of Ag^+ and fluorescence intensity in the range of 0–2.0 equiv. with a detection limit of 1 nM, which matches the requirements for analysis and monitoring of drinking water with the standards of World Health Organization (0.2–0.3 $\mu g\,L^{-1}$) (Fig. S6).

Similarly, a new, intense emission band around 528 nm appeared within 1 s when **1** was loaded with Zn^{2+} in CH_3CN–H_2O mixed solution (Fig. S14). Only the addition of Ca^{2+} had a slight interference. In contrast, the addition of Ag^+ did not show any changes in fluorescence intensity (Fig. 1b). The solution investigation demonstrated the similar results that the containing of 20% CH_3CN in the CH_3CN–H_2O mixed solution would be perfect for fluorescent detection. A minimum of 1 μM Zn^{2+} can be easily detected when 10 μM of **1** was present. With increasing Zn^{2+} concentrations, the fluorescence intensity saturated at 5.0 equiv. of Zn^{2+} (Fig. 2b). The linear relationship between the concentration of Zn^{2+} and fluorescence intensity at 528 nm demonstrated that **1** is well suitable for quantitative detection of Zn^{2+} (Fig. S7). The competition experiments (Fig. 1) were then performed by adding the competing ion to the solutions which contained **1** and Ag^+/Zn^{2+}. The results also indicated that both the detections of Ag^+ and Zn^{2+} were not significantly interfered by other ions, except for the fluorescent quenching caused by Cu^{2+} and Fe^{3+}.

The recognition mechanisms of the fluorescent changes were then studied. Binding analysis using Job's plot established a 1:2 stoichiometry between **1** and Ag^+ (Fig. S10) and a 1:1 binding stoichiometry between **1** and Zn^{2+} (Fig. S11). According to the pioneering reports of Tae and co-workers [34,35], an irreversible desulfurization reaction of thiosemicarbazide resulting in the formation of 1,3,4-oxadiazole was supposed to be caused by the addition of Ag^+ (Scheme 1). This triggered the opening of the spirolactam ring, resulting in a large fluorescence enhancement. The IR analysis showed the infrared absorption at 1612 cm^{-1}, 1311 cm^{-1} and 1020 cm^{-1}, which were investigated to be equivalent to the υ^{as} (C=N), υ^{as} (C—O—C) and υ^{s} (C—O—C), respectively,

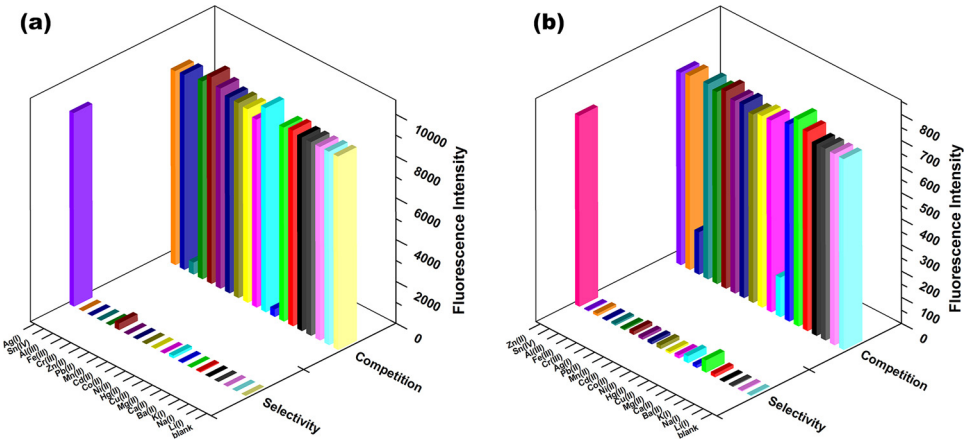

Fig. 1. Histogram showing selectivity and competition of **1** (10 μM) for Ag^+ (a) in EtOH–H_2O (2:8, v/v) solution and Zn^{2+} (b) in CH_3CN–H_2O (2:8, v/v) solution (PBS buffer, pH 7.4). The pillars in the front row represent fluorescence response of **1** to the metal ions of interest. The pillars in the back row represent the subsequent addition of 2 equiv. of Ag^+ (a) and 5 equiv. Zn^{2+} (b) to the solution containing **1** and the metal ions, respectively, λ_{ex} = 490 nm.

indicating the formation of the 1,3,4-oxadiazole ring (Fig. S26). This mechanism was also supported by the mass peak at *m*/*z* 476.1248 ($[M+H]^+$), which corresponds to the oxadiazole product **2** (calc. $C_{28}H_{17}N_3O_5$ for 475.1168). In contrast, the recognition of Zn^{2+} was proved to be reversible since the fluorescence intensity decreased when EDTA was added to the solution of **1** with Zn^{2+} (Fig. S15). The mass spectrum manifested the peak at *m*/*z* 608.0027, assigned as $[\mathbf{1}+Zn^{2+}+Cl^-]^+$, providing a powerful evidence for the binding mode of **1** with Zn^{2+}. Thus, several possible structures of the complex were reasonably proposed and theoretically optimized at DFT level with B3LYP functional [36,37]. The most probable structure **3** which was proposed and validated to has the lowest energy compared to others with the absence of imaginary frequencies (Fig. S29). This clearly indicated that Zn^{2+} bound with the O atom and N atom of the spirolactam moiety and the S atom of the benzoylthiourea moiety inducing the ring-opening process accompanied by the fluorescent changes (Scheme 1).

Calculations at the TDDFT [38–41] level based on the optimized structures of the ground S_0 state and the first excited S_1 state were performed to investigate the absorption and fluorescent emission of the ring-opened compounds **2** and **3** for verification of the proposed mechanism (Fig. 3). For both compounds, the absorption and emission corresponded mainly to the orbital transition between HOMO and LUMO. Take product **2** for example, the main absorption was observed from S_0 state to S_1 state (HOMO-LUMO, 410.26 nm) with the oscillator strength of 0.5378. The geometry relaxation between the S_0 state and the S_1 state greatly affected the energy level of the molecular orbitals, resulting in a 0.36 eV stabilization for the LUMO at the S_1 state geometry compared to that at the S_0 state geometry. As a result, the energy gap between the HOMO and LUMO is greatly decreased. The geometry relaxation was also proposed to be the main origin of the large Stokes shift for **2**, which is in agreement with the Jablonski-diagram of the fluorescence. A similar process was also observed for **3** with a 0.28 eV stabilization for the LUMO. The calculated emissions for **2** and **3** were 540.3 nm and 539.7 nm, respectively. The calculated emissions were found to be in significant agreement with the experimental value along with the observation of strong fluorescence, thus providing a powerful evidence for the proposed mechanism.

To evaluate the practical application of **1** for sensing Ag^+ and Zn^{2+} in living cells, the probe was cultured with Human Osteosarcoma MG-63 cells for 30 min at 37 °C (Fig. 4). Fluorescence microscopy images demonstrated that no fluorescence could be monitored. However, prominent fluorescent increases were observed when the cells were successively treated with Ag^+ and Zn^{2+}. Moreover,

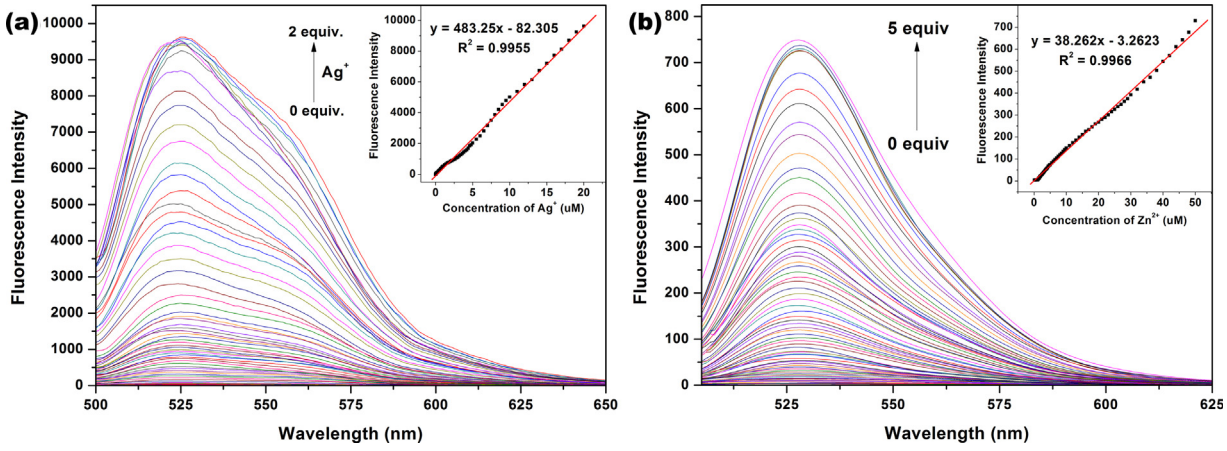

Fig. 2. Fluorescence intensity changes of **1** (10 μM) upon addition of Ag^+ (a) in EtOH–H_2O (2:8, v/v) solution and Zn^{2+} (b) in CH_3CN–H_2O (2:8, v/v) solution with PBS buffer (0.2 M, pH 7.4). Inset: linear relationship between the fluorescence intensity of **1** (10 μM) and the concentration of Ag^+ and Zn^{2+} at 525 nm and 528 nm, respectively, λ_{ex} = 490 nm.

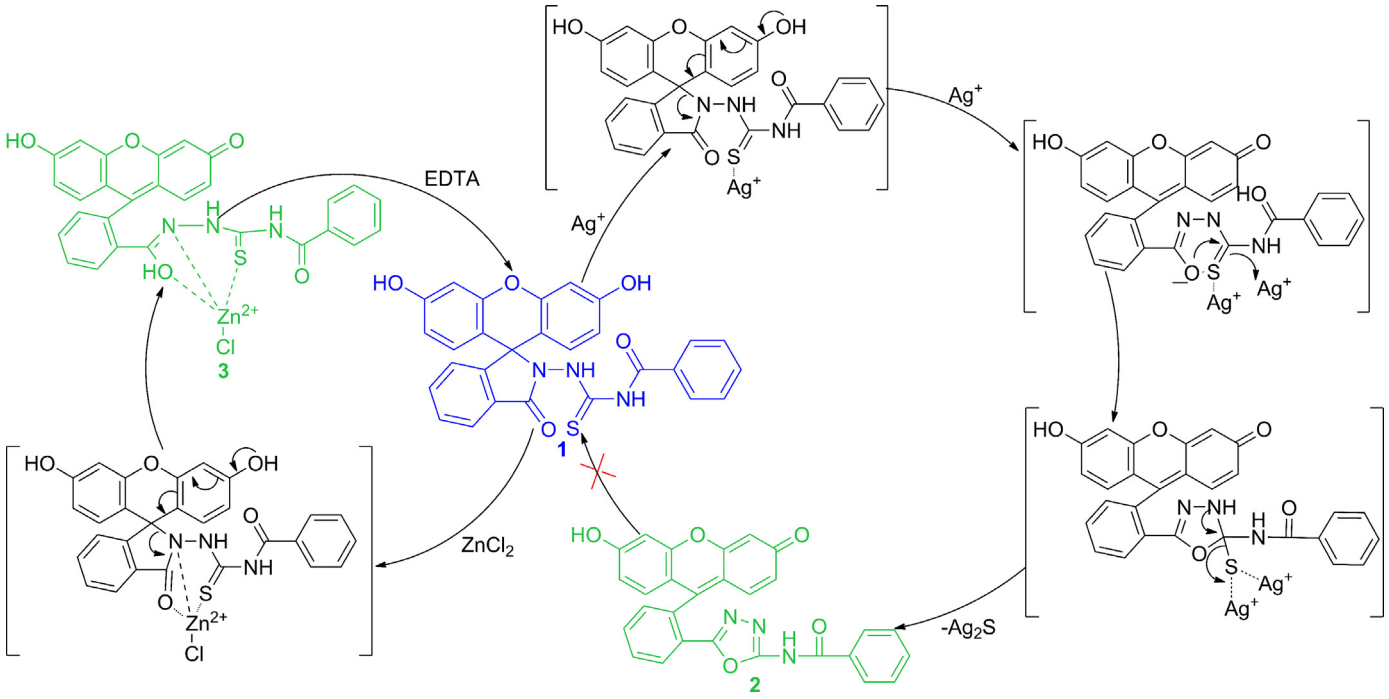

Scheme 1. Proposed recognition process for the fluorescent changes of **1** upon addition of Ag^+ and Zn^{2+}.

the cell morphology remained in good condition throughout the imaging experiments, indicating the low toxicity and great cytocompatibility of **1**. In addition, the overlay of fluorescent and bright-field images confirmed that the fluorescent signals were localized in the perinuclear area of the cytosol. Accordingly, the preliminary investigation suggested that probe **1** was cell membrane permeable and can be efficiently used for tracking Ag^+ and Zn^{2+} in living cells.

Probe **1** was then further used to localize Ag^+ and Zn^{2+} in microbial cell–EPS–mineral aggregates formed by the photosynthetic Fe(II)-oxidizing *Rhodobacter* sp. strain SW2 [33,42] through a multiple labeling method in combination with confocal laser scanning microscopy (Fig. 5). Probe **1**, SYTO® 9 green fluorescent nucleic acid stain and polysaccharide-specific Wheat germ agglutinin, Alexa Fluor® 633 conjugate were applied to stain Ag^+/Zn^{2+}, bacterial cells and extracellular polymeric substances, respectively. The fluorescence images indicate that Ag^+ and Zn^{2+} is collocated with bacterial cells, which seem to provide binding sites for Ag^+ and Zn^{2+}. The results furthermore show that probe **1** can be used to visualize Ag^+ and Zn^{2+} in microbial cell–EPS–mineral

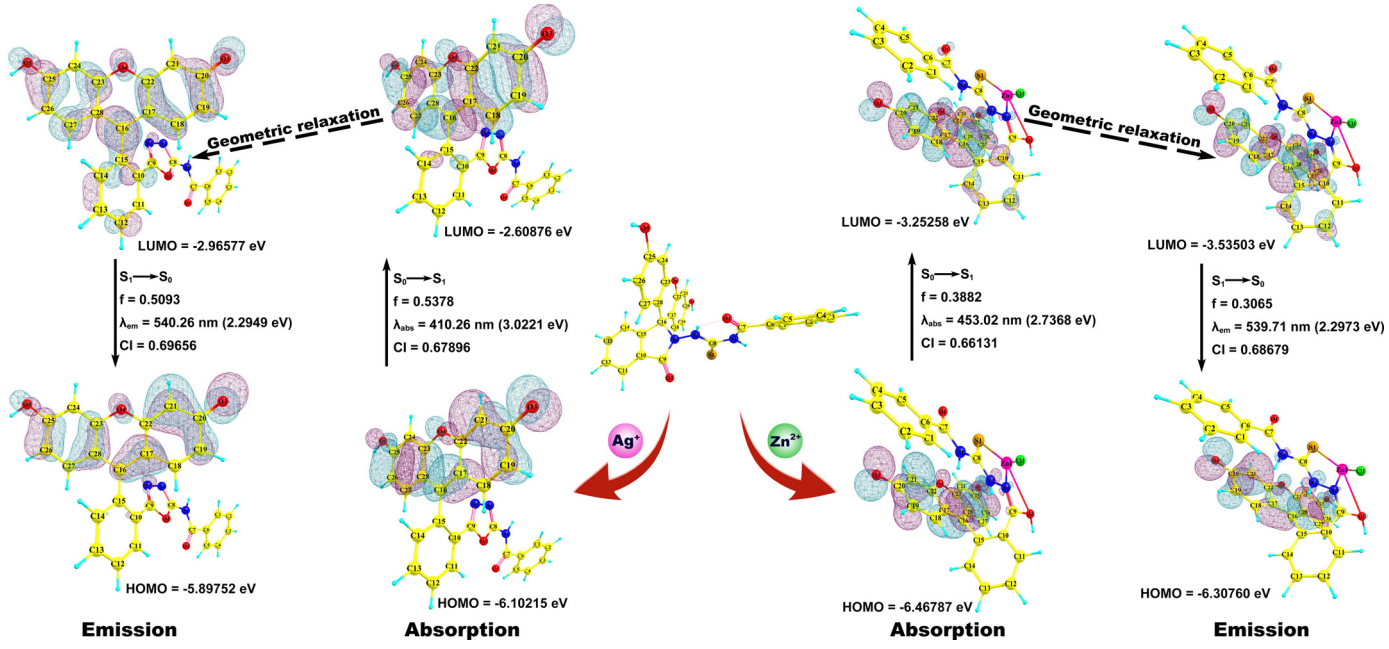

Fig. 3. Theoretical molding of the recognition process, wavelength (λ), excitation energy, oscillator strength (*f*), relevant frontier MOs (3D distribution and orbital energy), and corresponding CI coefficient of the absorption and emission of **2** and **3** at the TDDFT level based on the optimized structures of the ground S_0 state and the first excited S_1 state of compounds **2** and **3**.

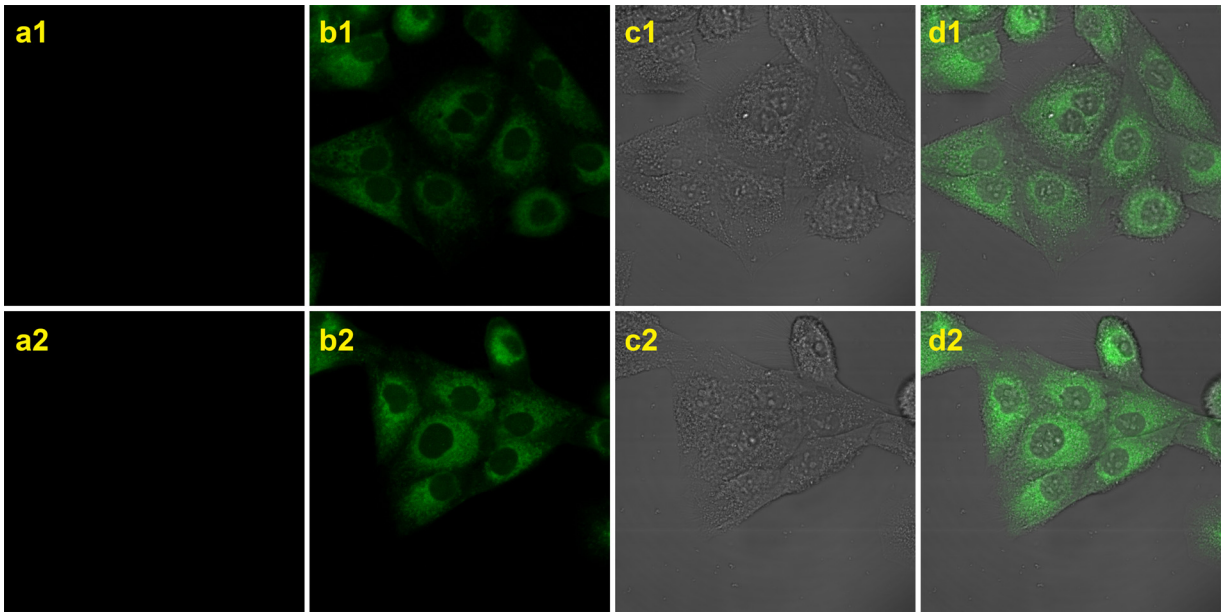

Fig. 4. Fluorescent imaging of **1** incubated with $AgNO_3$ and 8% C_2H_5OH (a1–d1) or $ZnCl_2$ and 8% CH_3CN (a2–d2), λ_{ex} = 488 nm, λ_{em} = 515–545 nm. (a) Human osteosarcoma MG-63 cells incubated with 10 μM of **1** for 30 min at 37 °C; (b) the cells successive incubated with 2 equiv. of Ag^+ and 8% C_2H_5OH or 5 equiv. Zn^{2+} and 8% CH_3CN in the same condition; (c) bright-field transmission image of the cells treated with probe **1** and Ag^+/Zn^{2+}; and (d) the overlay of the fluorescent and bright-field images.

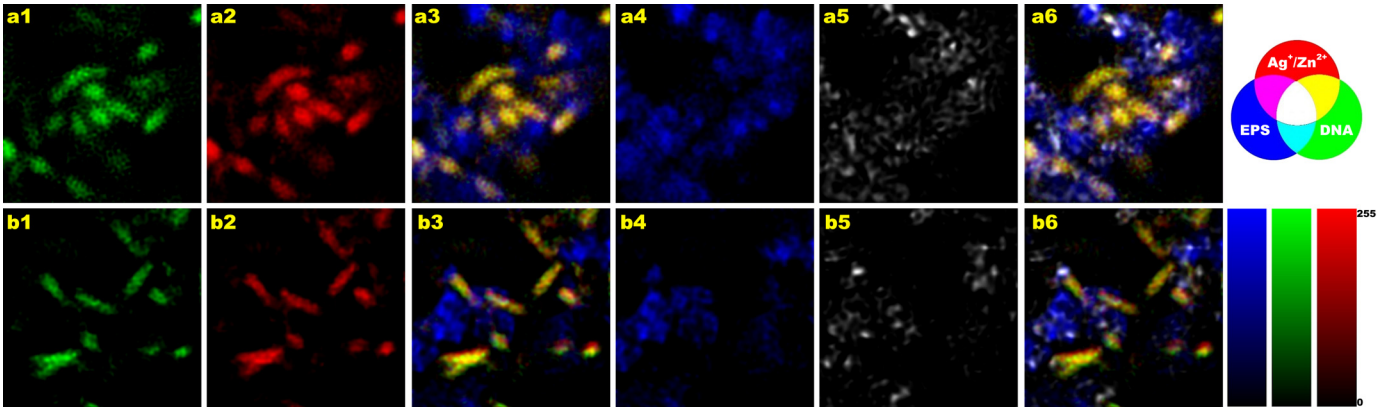

Fig. 5. Single cell scale map of the sorption of Ag^+ and Zn^{2+} to cell–EPS–mineral aggregates formed by Fe(II)-oxidizing *Rhodobacter* sp.strain SW2, incubated with 50 μM $AgNO_3$ and 8% C_2H_5OH (a1–a6) or 50 μM $ZnCl_2$ and 8% CH_3CN (b1–b6) for 1 h at 25 °C. The aggregate was simultaneously incubated with 50 μM probe **1** (2), fluorescent nucleic acid stain (1) and lectin conjugate (4) for 1 h at 25 °C, bacteriogenic minerals are visualized by their reflection signal (5) (λ_{ex} = 488 nm, 561 nm, 635 nm). The overlay image of (1) (2) and (4) is shown in (3); the overlay image of all four signals is shown in (6). Brighter color indicates higher metal concentrations. Scalebar: 1 μm.

aggregates close to natural and hydrated conditions, while solvent switch creates a controllable way to simultaneously track metals changes from Ag^+ to Zn^{2+} or Zn^{2+} to Ag^+ on the same interesting sample's spot especially with a flow chamber.

4. Conclusion

In summary, we present the design, synthesis and photophysical properties of a novel, solvent-dependent fluorescein–benzoylthiourea based probe which displayed specific selective "off–on" responses to Ag^+ in EtOH–H_2O (2:8, v/v) solution and to Zn^{2+} in CH_3CN–H_2O (2:8, v/v) solution. As indicated by combined experimental and theoretical study, the Ag^+ promoted desulfurization of thiosemicarbazide functionality in formation of the 1,3,4-oxadiazole and the coordination of Zn^{2+} to the O atom and N atom of the spoirolactam moiety and the S atom of the benzoylthiourea moiety reasonably promoted the fluorescent enhancement. Probe **1** provides a promising candidate for bioleaching studies of visualizing Ag^+ and Zn^{2+} in living cells and microbial cell–EPS–mineral aggregates, which may contribute to significant breakthroughs in understanding the correlation between the metals and related cells and organic substances.

Acknowledgements

We thank Prof. Dr. A. Kappler, Prof. Z. Shi, F. Zeitvogel, P. Ingino and G. Schmid for their great helpful support. We are grateful for the support from the NSF of China (Nos. 21272184, 21103137, 20972124 and J1210057), the Shaanxi Provincial Natural Science Fund Project (No. 2012JQ2007), the Science and Technology Project of Xi'an City (Nos. CXY1429(6), CXY1434(7)), the Northwest University Science Foundation for Postgraduate Students (Nos. YZZ12030 and YZZ13042) and the Emmy-Noether Fellowship Program of the DFG to M.O. (OB 362/1-1).

Appendix A. Supplementary data

Supplementary data associated with this article can be found, in the online version, at http://dx.doi.org/10.1016/j.aca.2015.01.052.

References

[1] X.H. Li, X.H. Gao, W. Shi, H.M. Ma, Chem. Rev. 114 (2014) 590–659.
[2] Z.Q. Guo, S. Park, J. Yoon, I. Shin, Chem. Soc. Rev. 43 (2014) 16–29.
[3] K. Zscharnack, T. Kreisig, A.A. Prasse, T. Zuchner, Anal. Chim. Acta 834 (2014) 51–57.
[4] S. Goswami, A.K. Das, A. Manna, A.K. Maity, P. Saha, C.K. Quah, H. Fun, H.A. Abdel-Aziz, Anal. Chem. 86 (2014) 6315–6322.
[5] M. Yamanaka, K. Hara, J. Kudo, Appl. Environ. Microbiol. 71 (2005) 7589–7593.
[6] K. Chun, Y. Oh, J. Rho, J. Ahn, Y. Kim, H.R. Choi, S. Baik, Nat. Nanotechnol. 5 (2010) 853–857.
[7] C.J. Frederickson, J. Koh, A.I. Bush, Nat. Rev. Neurosci. 6 (2005) 449–462.
[8] J. Koh, S.W. Suh, B.J. Gwag, Y.Y. He, C.Y. Hsu, D.W. Choi, Science 272 (1996) 1013–1016.
[9] A. Chatterjee, M. Santra, N. Won, S. Kim, J.K. Kim, S.B. Kim, K.H. Ahn, J. Am. Chem. Soc. 131 (2009) 2040–2041.
[10] Z.C. Xu, J. Yoon, D.R. Spring, Chem. Soc. Rev. 39 (2010) 1996–2006.
[11] Z.C. Xu, K. Baek, H.N. Kim, J. Cui, X.H. Qian, D.R. Spring, I. Shin, J. Yoon, J. Am. Chem. Soc. 132 (2010) 601–610.
[12] R.J. Radford, W. Chyan, S.J. Lippard, Chem. Sci. 4 (2013) 4532–4533.
[13] S. Goswami, A.K. Das, K. Aich, A. Manna, S. Maity, K. Khanra, N. Bhattacharyya, Analyst 138 (2013) 4593–4598.
[14] J.F. Zhang, Y. Zhou, J. Yoon, J.S. Kim, Chem. Soc. Rev. 40 (2011) 3416–3429.
[15] M.M. Hu, J.L. Fan, J.F. Cao, K.D. Song, H. Zhang, S.G. Sun, X.J. Peng, Analyst 137 (2012) 2107–2111.
[16] F. Cheng, E.M. Bonder, F. Jakle, J. Am. Chem. Soc. 135 (2013) 17286–17289.
[17] S.X. Chen, D.Y. Zhang, G. Seelig, Nat. Chem. 5 (2013) 782–789.
[18] X.F. Yang, Y.X. Guo, R.M. Strongin, Angew. Chem. Int. Ed. 50 (2011) 1–50.
[19] H.Y. Zhang, Z.F. Li, A. Snyder, J. Xie, L.A. Stanciu, Anal. Chim. Acta 827 (2014) 86–94.
[20] L.N. Neupane, J. Park, J.H. Park, K. Lee, Org. Lett. 15 (2013) 254–257.
[21] G.C. Zhu, Y. Li, C.Y. Zhang, Chem. Commun. 50 (2014) 572–574.
[22] Y.L. Liu, Y. Sun, J. Du, X. Lv, Y. Zhao, M.L. Chen, P. Wang, W. Guo, Org. Biomol. Chem. 9 (2011) 432–437.
[23] L. Xu, Y.F. Xu, W.P. Zhu, B.B. Zeng, C.M. Yang, B. Wu, X.H. Qian, Org. Biomol. Chem. 9 (2011) 8284–8287.
[24] X.Q. Chen, T. Pradhan, F. Wang, J.S. Kim, J. Yoon, Chem. Rev. 112 (2012) 1910–1956.
[25] M.L. Zhao, X.F. Yang, S.F. He, L.P. Wang, Sens. Actuators B 135 (2009) 625–631.
[26] H.B. Yu, Y. Xiao, H.Y. Guo, X.H. Qian, Chem. Eur. J. 17 (2011) 3179–3191.
[27] L.J. Tang, Y. Li, R. Nandhakumar, J.H. Qian, Monatsh. Chem. 141 (2010) 615–620.
[28] Z. Yang, M.J. Wang, M.Y. She, Y.Y. Huang, B. Yin, P. Liu, J.L. Li, S.Y. Zhang, Sens. Actuators B 202 (2014) 656–662.
[29] J.P. Perdew, K. Burke, M. Ernzerhof, Phys. Rev. Lett. 77 (1996) 3865–3868.
[30] M.J. Frisch, G.W. Trucks, H.B. Schlegel, G.E. Scuseria, M.A. Robb, J.R. Cheeseman, G. Scalmani, V. Barone, B. Mennucci, G.A. Petersson, H. Nakatsuji, M. Caricato, X. Li, H.P. Hratchian, A.F. Izmaylov, J. Bloino, G. Zheng, J.L. Sonnenberg, M. Hada, M. Ehara, K. Toyota, R. Fukuda, J. Hasegawa, M. Ishida, T. Nakajima, Y. Honda, O. Kitao, H. Nakai, T. Vreven, J.A. Montgomery Jr., J.E. Peralta, F. Ogliaro, M. Bearpark, J.J. Heyd, E. Brothers, K.N. Kudin, V.N. Staroverov, R. Kobayashi, J. Normand, K. Raghavachari, A. Rendell, J.C.S. Burant, S. Iyengar, J. Tomasi, M. Cossi, N. Rega, J.M. Millam, M. Klene, J.E. Knox, J.B. Cross, V. Bakken, C. Adamo, J. Jaramillo, R. Gomperts, R.E. Stratmann, O. Yazyev, A.J. Austin, R. Cammi, C. Pomelli, J.W. Ochterski, R.L. Martin, K. Morokuma, V.G. Zakrzewski, G.A. Voth, P. Salvador, J.J. Dannenberg, S. Dapprich, A.D. Daniels, O. Farkas, J.B. Foresman, J.V. Ortiz, J. Cioslowski, D.J. Fox, Gaussian 09, Revision A.02, Gaussian, Inc., Wallingford, CT, 2009.
[31] Z. Yang, M.Y. She, J. Zhang, X.X. Chen, Y.Y. Huang, H.Y. Zhu, P. Liu, J.L. Li, S. Shi, Sens. Actuators B Chem. 176 (2013) 482–487.
[32] F. Hegler, N.R. Posth, J. Jiang, A. Kappler, FEMS Microbiol. Ecol. 66 (2008) 250–260.
[33] Z. Yang, L.K. Hao, B. Yin, M.Y. She, M. Obst, A. Kappler, J.L. Li, Org. Lett. 15 (2013) 4334–4337.
[34] Y. Yang, K. Yook, J. Tae, J. Am. Chem. Soc. 127 (2005) 16760–16761.
[35] S. Ko, Y. Yang, J. Tae, I. Shin, J. Am. Chem. Soc. 128 (2006) 14150–14155.
[36] R.G. Parr, W. Yang, Density Functional Theory of Atoms and Molecules, Oxford University Press, New York, 1989.
[37] A.D. Becke, J. Chem. Phys. 98 (1993) 5648–5652.
[38] E. Runge, E.K. Gross, Phys. Rev. Lett. 52 (1984) 997–1000.
[39] J.Y. Shao, H.Y. Sun, H.M. Guo, S.M. Ji, J.Z. Zhao, W.T. Wu, X.L. Yuan, C.L. Zhang, T. D. James, Chem. Sci. 3 (2012) 1049–1061.
[40] Y.H. Chen, J.Z. Zhao, H.M. Guo, L.J. Xie, J. Org. Chem. 77 (2012) 2192–2206.
[41] Z. Yang, M.Y. She, B. Yin, J.H. Cui, Y.Z. Zhang, W. Sun, J.L. Li, Z. Shi, J. Org. Chem. 77 (2012) 1143–1147.
[42] L.K. Hao, J.L. Li, A. Kappler, M. Obst, Appl. Environ. Microbiol. 79 (2013) 6524–6534.